Optimal Design of PV/WT/Battery Based Microgrid for Rural Areas in Leh Using Dragonfly Algorithm

Subhash Yadav*, Pradeep Kumar and Ashwani Kumar

National Institute of Technology, Kurukshetra, Haryana, India
E-mail: subhash05754@gmail.com; pradeepkumar@ieee.org;
ashwani.k.sharma@nitkkr.ac.in
*Corresponding Author

Abstract

This study proposes an optimal microgrid design for rural electrification in India's Leh and Ladakh regions, using wind energy, solar, energy, and battery energy storage system. The Dragonfly Algorithm (DA) is used to calculate the optimal number of microgrid units, and results are compared with popular optimization algorithms such as Grey Wolf optimization (GWO), Differential Evolution (DE), and Discrete Harmony Search (DHS). The optimal design is based on an objective function to minimize the Levelized cost of energy (LCOE) while keeping the loss of power supply probability (LOPSP) as a reliability constraint. Three configuration studies are carried out, with three cases, each with a different maximum permissible LOPSP ($LOPSP^{max}$) value. The results show that optimal design and efficient energy management reliably meet the load demand. The energy generated from the proposed microgrid is clean compared to the grid supply, and the amount of greenhouse gas (GHG) emissions is reduced by 91.2% from Configuration-I, Case-I, which is the most economical configuration. The LCOE obtained

from Configuration-I, Case-I is 0.129 \$/kWh, the lowest among similar systems available in the literature. To determine the parameter cost with supply, the LCOE and Total life cycle cost (TLCC) sensitivity to $LOPSP^{max}$ are considered. Furthermore, statistical analysis shows that DA outperforms GWO, DE, and DHS in terms of accuracy and convergence rate.

Keywords: Photovoltaic, wind energy, battery energy storage, greenhouse gas emissions, microgrid, levelized cost of energy.

Nomenclature

Symbol	Name
BESS	Battery energy storage system
BSO-OS	Brainstorm optimization in objective space
COE	Cost of Energy
CSP	Concentrated solar power system
DG	Diesel Generator
FC	Fuel cell
FPA	Flower pollination algorithm
HGWOSCA	Grey wolf optimizer-sine-cosine algorithm
LCOE	Levelized cost of energy
MFO	Moth flame optimization
MOEA/D	Multi-objective evolutionary algorithm based on decomposition
NPC	Net present cost
NSGA	Non-dominated shorted GA
PHS	Pump storage plant
PSO	Particle swarm optimization
PV	Photovoltaic
SA	Simulated annealing
SCA	Sine cosine algorithm
SPEA-II	Strength Pareto evolutionary algorithm
S-SSA	Simplified squirrel search algorithm
TES	Thermal energy storage
TNPC	Total net present cost
WT	Wind energy generation
Ah	Battery Amp-hour
CP_r	Capital cost of rth component in \$

Symbol	Name
$G_h(t)$	Solar irradiation incident at the horizontal surface at t hour in kW/m^2
i	Interest rate
INT(.)	Function used to return the smallest integer number
L_r	Complete lifetime of rth component in year
L_p	Complete lifetime of the project in the year
N_r	The number of components
L_r^{rem}	Surplus life of rth component in year
N_{bat}	Number of batteries
NC	Component used in microgrid
OM$_{npv,r}$	Maintenance cost of rth component in $
$P_{ext}(t)$	Generated excess power supplied to the dummy load in t hour in kW
P_{inv}^R	Rated power of the inverter
RP$_{npv,r}$	Replacement cost of rth component in $
R_r^{rp}	Last replaced time of rth components
SV$_{npv,r}$	Salvage value of the rth component in $
α_r	Initial capital cost of components in $/unit
β_r	Operation and maintenance cost of components in $/unit/year
ξ_r	Replacement cost of components in $/unit
λ_r	Resale price of rth components
δ	Inflation rate
γ	Escalation rate

1 Introduction

Microgrids have solved the problem of rural electrification in several Asian and African countries, where grid-connection is difficult and uneconomical [1]. The renewable energy source (RES)-based microgrids have provided clean and affordable energy sources in several remote locations [2–6]. The availability of energy sources in the area influences the choice of energy sources for the microgrid. Table 1 summarizes the literature's various hybrid energy system configurations, optimization algorithms, operation modes, locations, and objectives. The primary concern in these areas is an economical operation using various optimization algorithms. The energy storage systems (ESS) and the reliability index loss of power supply probability (LOPSP) are used to assess system reliability [7–10].

Table 1   Literature review of different studies

Ref.	Algorithm	Configuration	Mode	Location	Objectives
[8]	Multi-objective genetic algorithm (MOGA)	PV/ WT/BESS	Isolated	Rabat, Morocco	Minimizes Levelized cost of energy (LCOE) and maximizes power supply reliability.
[9]	Harmony search (HS), Jaya, and PSO.	WT /PV/ Biomass/BESS	Isolated	Saudi Arabia	Cost minimization, maximum allowable LOPSP, and reducing allowable excess energy fraction.
[10]	PSO	PV/BESS/ PHS	Isolated	Ipoh, Malaysia	Minimize the Cost of energy (COE) at LOPSP 0%.
[11]	NSGA-II, MOPSO, MOEA/D, SPEA-II	PV/WT/BESS/ PHS/ hydrogen/ thermal ESS	Isolated	Karachi, Pakistan	Minimizing economy, LCOE and Improving reliability, LOPSP.
[12]	NSGA-II	WT/BESS/FC/ supercapacitor	Isolated	Tanda, Ivory coast	Optimal sizing and minimization of the total annual cost considering LOPSP.
[13]	Firefly algorithm (FA)	PV/ WT/FC	Grid-connected	Hurghada, Egypt	Optimal sizing, minimizing Total net present cost (TNPC) considering LOPSP as reliability index.
[14]	Multi-objective PSO (MOPSO)	PV/WT/BESS	Grid-connected	Ismailia Governorate, Egypt	Minimizes LOPSP, COE and maximizes RES fraction.
[15]	MOPSO	PV/WT/DG/ hydroki- netic/BESS	Isolated	Sub-Saharan Africa	Minimize the LOPSP, COE, total emission, and diesel contribution factor.
[16]	Genetic algorithm (GA)	PV/ WT /BESS	Isolated	Jeju Island, South Korea	Optimal Sizing, Capacity fading, temperature variation, and sensitivity study of RES penetration.
[17]	HOMER software	PV/WT/BESS/FC	Isolated	South Africa and Nigeria	Minimize the TNPC and calculate LCOE.
[18]	Hybrid GA with PSO and MOPSO	PV/ WT /BESS	Isolated	Tehran	Minimize TNPC and maximize reliability for the off-grid residential load.
[19]	PSO, GA, FA, and Ant colony optimization	WT/ PV/BESS/ PHS	Isolated	Island Jiuduansha, China	Minimize net present cost (NPC).
[20]	Teaching learning based optimization (TLBO)	PV/BESS	Grid-connected	Iran	Minimize the TNPC and evaluate COE.
[21]	HOMER software	PV/WT/DG/BESS	Isolated	India	Optimal design and minimize NPC and calculate COE.

<div align="right">(Continued)</div>

Table 1 Continued

Ref.	Algorithm	Configuration	Mode	Location	Objectives
[22]	HGWOSCA, GWO, PSO and SCA	PV/WT/FC	Isolated	Iran	Optimal sizing and minimizing the life span cost of hybrid systems and load interruption probability.
[23]	GA, CS, SA, HS, Jaya, FA, FPA, MFO, BSO-OS, S-SSA	PV and WT/BESS	Isolated	Algeria	Minimize the TNPC, subject to deficiency of power supply probability.
[24]	Modified electric system cascade and power pinch analysis	PV/CSP/WT/TES /BESS	Isolated	Oujda, Morocco	Optimal sizing of hybrid system with multiple storage systems and Minimizing the LCOE by ensuring maximum load supply.
[25]	Improved Artificial Ecosystem Optimization (IAEO)	PV/WT/FC	Grid-connected, Isolated	Suez Gulf, Egypt	Minimize the COE, considering reliability index LOPSP and excess energy.
[26]	HOMER software	PV/WT/BESS/ Biomass	Isolated	Fars province, Iran	Minimize the NPC and calculate COE.
[27]	TRNSYS software	PV/WT/DG/BESS	Isolated	Konya, Turkey	Optimal design and dynamic simulation, Minimizing LCOE and CO_2 emissions.
[28]	FA, PSO, and Shuffled Frog Leaping algorithm	PV/WT/FC	Isolated	Egypt	Minimize the NPC, subject to LOPSP.
[29]	Fuzzy logic	PV/WT/BESS	Isolated	South Australia	Minimize NPC and optimal sizing using novel demand side management.
[30]	Hybrid Optimization of Multiple Energy Resources (HOMER) Pro	PV/WT/BESS/ Biomass	Isolated	China	Optimal designing of hybrid renewable energy system with minimizing NPC, and COE
[31]	HOMER Pro	PV/WT/BESS	Isolated	Cameroon	Techno-economic analysis, Minimizing NPC, COE

Based on the literature review conducted, it is realized that

- None of the studies consider the feasibility of wind energy generation at high altitudes where air density (δ_{ar}) is very low.
- Only a few authors [14] have considered and evaluated Greenhouse gas (GHG) emissions from renewable energy generation units and battery energy storage systems (BESS) due to life cycle procedures such as manufacturing, material transfers, assembly, system installation, and disposal or recycling.

- Limited studies been performed by applying the Dragonfly algorithm (DA) for optimal design of PV/WT/BESS based isolated microgrid.

As a result, the primary goal of this study is to optimally design a PV/WT/BESS to electrify rural/remote areas using distributed RES that are locally available at minimum Levelized cost of energy (LCOE), as well as feasibility and reliability studies of wind energy generation (WT) with solar photovoltaic (PV) and BESS at high altitudes. Using RES-based microgrids eliminates fossil fuel-based energy generation and GHG emissions, serious issues for global warming, the environment, and social and health safety. The following are the work's significant contributions:

- Optimal design of microgrid consisting of PV, WT, and BESS to minimize the LCOE in the study area using DA, comparing with popular metaheuristic algorithm GWO, DE, and DHS, and analysis of feasibility at low air density area (due to high altitude).
- Power supply reliability in isolated mode with LOPSP constraint.
- The algorithms are statistically analyzed for accuracy, robustness, and convergence rate.
- GHG emissions from microgrid components have been assessed and compared to grid supply.

The study is performed for 48 village hamlets in four blocks, Chuchat, Durbuk, Kharu, and Nyoma, of Leh district of Union Territory of Ladakh, India. There are no such studies in the literature for the site. Because of the area's slow electrification rate, development in Leh and the surrounding territories has been gradual [32]. Grid connectivity may be limited or non-existent due to difficult terrain and low population density [33]. According to [34, 35], the site has solar and wind energy potential. As a result, the primary energy sources chosen are solar energy and wind energy, both of which are operated with the combination of BESS. The Dragonfly algorithm (DA) [36], Grey Wolf optimization (GWO) [37], differential evolution (DE) [38], and discrete harmony search (DHS) [5, 39] are used to optimize the sizing of these sources.

These algorithms were chosen for their simple structure and ability to handle nonlinear optimization problems. These optimization techniques are examples of different meta-heuristics algorithms, such as DA and GWO for swarm intelligence, DE for evolutionary algorithms, and DHS for physics-based algorithms [40]. The primary objective of this paper is to reduce the LCOE. The ability of the generation system to meet the load requirement is assessed using the LOPSP reliability index [9]. LOPSP is the probability that

the available energy supply is insufficient to meet the load demand (P_L) [8]. Three different configurations are used for the study. Each configuration is evaluated with the maximum allowable LOPSP ($LOPSP^{max}$) of 0%, 2%, and 4%.

The rest of the paper is organized as follows: **Section 2** discusses the System Configuration. **Section 3** presents the mathematical model of the different energy sources used. Problem formulation is presented in **Section 4**. **Section 5** presents the different optimization algorithms used. Results are discussed in **Section 6**. Finally, the conclusions are drawn in **Section 7**.

2 System Configuration

2.1 Site Description

The study site is '*Chushul*,' located at 33° 35′11.9″N, 78° 38′35.8″E, with an elevation of 4510.4 m above sea level and a net altitude of 4560.4 m above sea level. It comprises of 48 village hamlets in four remote blocks of Leh district, India, with hilly terrain and extremely high altitudes [41]. Due to the difficult terrain and low population density, grid interconnections are difficult and uneconomical at these locations [42]. 'Chushul' has an annual average wind speed (v) = 6.6 m/s at 50 m above ground level, an annual average density of 0.7 kg/m^3, and an annual average daily solar irradiation (G_h) of 221.29 Watt/m^2 [35]. The site has high wind and solar potential [34]. As a result, RESs are a viable option for meeting energy demand. The monthly average hourly G_h and v data, as shown in Figures 1(a) and 1(b), and load variation pattern shown in Figure 1(c) shows a peak occurring between 20:00 and 23:00 hrs.

2.2 Microgrid Components

The proposed microgrid, depicted in Figure 2, comprises PV panels, a WT, a BESS system, AC electrical load, and dummy loads. The inverter, connected to the AC load, receives the DC output from the WT and PV. The BESS is linked to a DC bus. If the electric load is less than the generation, the BESS stores the surplus power, and vice versa. The excess power (P_{ext}) is feed to the dummy load if BESS is fully charged. Cost minimization is achieved while meeting load demand with these sources. Table B1 (Appendix B) shows the technical specifications of the inverter [43], PV panel [43–45], WT [43, 44], BESS (lead acid type, 24 V and 150 Ah) [44] used to calculate the generating and storage units.
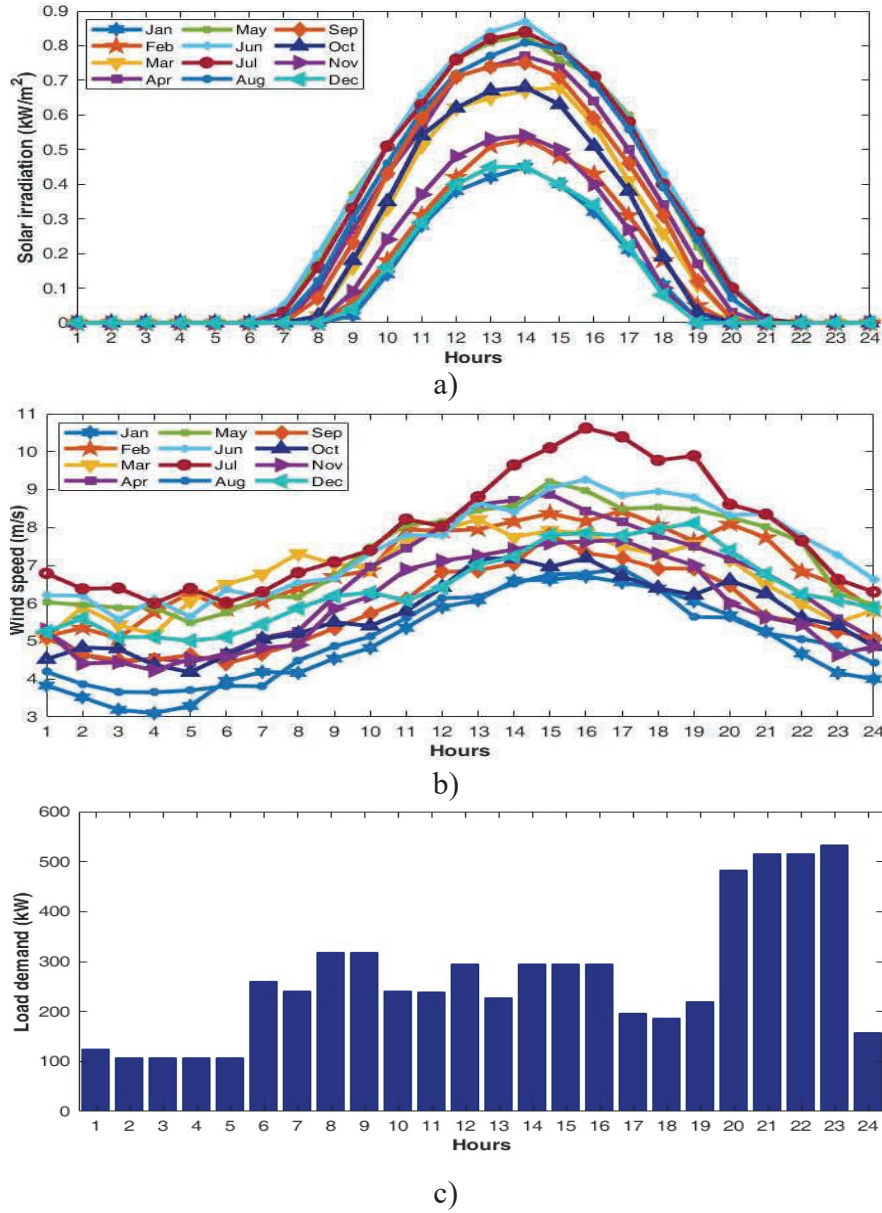
Figure 1   Waveforms of the a) Monthly average hourly solar irradiation, b) Monthly average hourly wind speed, and c) Hourly load profile.
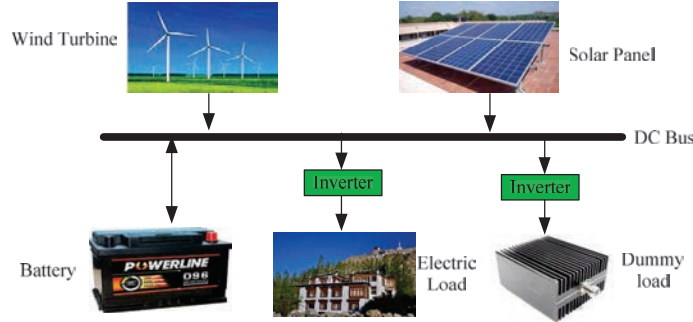
Figure 2 Layout of the proposed microgrid.

3 Mathematical Modeling

The mathematical model of microgrid components is discussed below:

3.1 Solar Photovoltaic

The total output power from the PV panel $P_{PV,T}$ is given as [43]:

$$P_{PV,T}(t) = N_{PV} \times P_{PV}^r \times d_{Loss} \times (G_h(t)/G_{STC}) \tag{1}$$

where, N_{PV} is the number of PV panels, d_{Loss} is the derating factor, G_h represents solar irradiation, G_{STC} refers to solar irradiation at standard temperature conditions, P_{PV}^r indicates the rated power of a PV panel, and N_{PV} is the number of PV panels.

The derating or loss factor of the PV panel, d_{Loss} accounts for the aging factor, shadow formation and dust deposition over the PV panel surface, etc.

3.2 Wind Turbine

The total output power from the WT, $P_{WT,T}$, is calculated as follows:

$$P_{WT,T}(t) = N_{WT} \times P_{WT}(t) \tag{2}$$

where, N_{WT} is the number of WT, and P_{WT} is the power generated by the WT given as [44, 46, 47]:

$$P_{WT}(t) = \begin{cases} 0 & 0 \leq v(t) \leq v_{Cin} \ \& \ v(t) \geq v_{Cof} \\ P_{RW}\dfrac{v^3(t) - v_{Cin}^3}{v_{Rt}^3 - v_{Cin}^3} & v_{Cin} < v(t) < v_{Rt} \\ P_{RW} & v_{Rt} \leq v(t) < v_{Cof} \end{cases} \tag{3}$$

where, P_{RW} is the rated power WT, v_{Cin}, v_{Rt}, and v_{Cof} are cut-in, rated and cut-off wind speed.

3.3 Battery Energy Storage System

BESS stores the surplus energy when total renewable power generation $(P_{\text{Res},T})$ is more than P_L and discharges the stored energy whenever $P_{\text{Res},T} < P_L$, to meet the P_L. The charging and discharging of the battery are described below. In each case, the charging or discharging is decided by the $P_{\text{Res},T}, P_L$, and state of charge (SOC) of the BESS [11, 18, 20].

Charging: If $P_{\text{Res},T}(t) \geq (P_L(t)/\eta_{inv})$, and SOC(t) $\leq$ SOC$^{\text{max}}$ (Maximum value of *SOC*) [11] BESS stores the energy. Then,

$$SOC(t) = SOC(t-1) \times (1 - \lambda) + (P_{\text{Res},T}(t)$$
$$- (P_L(t)/\eta_{inv})) \times \eta_{bcg} \qquad (4)$$

where, λ refers to the hourly self-discharge rate, η_{bcg} represents the charging efficiency of the battery and η_{inv}, indicates the efficiency of the inverter.

If $SOC(t) = SOC^{max}$, BESS is fully charged and $P_{ext}(t)$ feeds the dump load, [9, 48]. The $P_{ext}(t)$ is calculated as Equation (5)

$$P_{ext}(t) = P_{\text{Res},T}(t) - (P_L(t)/\eta_{inv}) - (SOC^{\text{max}} - SOC(t-1)$$
$$\times (1 - \lambda)) \times \eta_{bcg} \qquad (5)$$

Discharging: If $P_{\text{Res},T}(t) \leq (P_L(t)/\eta_{inv})$ and SOC(t) $>$ SOC$^{\text{min}}$ (Minimum value of *SOC*), BESS feeds the load, and its SOC is

$$SOC(t) = SOC(t-1) \times (1 - \lambda) - ((P_L(t)/\eta_{inv})$$
$$- P_{\text{Res},T}(t))/\eta_{bdg} \qquad (6)$$

where, η_{bdg} represents discharging efficiency of the battery.

The SOC^{min} depends on the DOD of the BESS [11, 49]. If $SOC(t)$ becomes less than SOC^{min} during this process, then a fraction of the load is not supplied, and set $SOC(t) = SOC^{min}$. The loss of power supply (LOPS) is calculated as [44]:

$$LOPS(t) = (P_L(t)/\eta_{inv}) - P_{\text{Res},T}(t) - [SOC(t-1)$$
$$\times (1 - \lambda) - SOC^{\text{min}}] \times \eta_{bdg} \qquad (7)$$

3.4 Inverter

The inverters convert the DC output power of PV, WT, and BESS into AC to feed the AC loads. The total inverter capacity $(P_{inv,T})$ depends on peak load demand $(P_{L,Peak})$ [43], and the number of inverters (N_{inv}), is calculated as follows:

$$P_{inv,T}(t) = P_{L,Peak}(t)/\eta_{inv} \tag{8}$$

$$N_{inv} = P_{inv,T}(t)/P_{inv}^R \tag{9}$$

where, P_{inv}^R is the rated capacity of the inverter.

3.5 Life Cycle Cost

Using the life cycle cost (LCC), the cost analysis is performed for the proposed microgrid. LCC analysis calculates the net present value (npv) of all the expected expenses over the system life span. The LCC of the rth component, LCC_r, is given as (10), and the cost components can be evaluated as (11)–(16) [10, 14, 50]:

$$LCC_r = CP_r + OM_{npv,r} + RP_{npv,r} - SV_{npv,r} \tag{10}$$

$$CP_r = \alpha_r \times N_r \tag{11}$$

$$OM_{npv,r} = \beta_r \times N_r \times \sum_{j=1}^{L_P}((1+\gamma)/(1+i))^j \tag{12}$$

$$RP_{npv,r} = \xi_r \times N_r \times \sum_{k=1}^{INT[(L_p/L_r)]-1}((1+\delta)/(1+i))^{k \times L_r} \tag{13}$$

$$R_r^{rp} = L_r \times INT(L_p/L_r) \tag{14}$$

$$L_r^{rem} = L_r - (L_p - R_r^{rp}) \tag{15}$$

$$SV_{npv,r} = \lambda_r \times N_r \times (L_r^{rem}/L_r) \times ((1+\delta)/(1+i))^{L_p} \tag{16}$$

where, δ, is the inflation rate, i represents the interest rate, γ refers to escalation, L_p represents project lifetime, α_r is the initial capital cost of components, β_r shows the operation and maintenance cost of components, λ_r indicates the resale price of components and ξ_r is the replacement cost of components.

Total LCC (TLCC) of the microgrid includes LCC of PV, WT, BESS, and inverter. To convert the TLCC into annual cost, capital recovery factor (CRF) is used (17) [10, 19]. It is considered that the power generated by RES is the same every year till the project's lifetime. The LCOE is defined as (18) [10, 19, 50]:

$$CRF(i, L_p) = (i(1+i)^{L_p}/((1+i)^{L_p} - 1)) \tag{17}$$

$$LCOE = CRF(i, L_p) \times \left(\sum_{r \in NC} LCC_r \Big/ \sum_{t=1}^{T=8760} P_L(t) \right) \tag{18}$$

3.6 Greenhouse Gas (GHG) Emission

RESs generate clean energy, meaning they don't emit GHGs while operating. However, their production, material transfer, assembly, system installation, and disposal or recycling emit significant amounts of GHG. Because of the properties of the emitted gases, the GHGs emitted from different units have different effects on global warming. All emissions are referred to as CO_2 equivalents (CO_2-eq) to compare the GHG effect of various gases. The CO_2-eq is a measuring scale in which CO_2 is the reference point and has a global warming potential (GWP) of 1, and other GHGs have a GWP greater than CO_2. Methane (CH_4), Nitrous oxide (N_2O), and Sulfur hexafluoride (SF_6) have GWPs of 21, 310, and 23900, respectively [14, 51]. To compare GHG emissions for the proposed system, the base case is the load supplied from the grid, which comprises thermal energy sources. The grid's GHG emissions are given as follows:

$$GHG_{grid} = P_L \; supplied \; by \; grid \; \times grid_{esf} \times GWP \tag{19}$$

where $grid_{esf}$ is electricity specific factor whose value in India is 1.3332 (kgCO$_2$-eq/kWh) [52].

The GHG emission from a PV system (E_{PV}) is calculated as:

$$E_{PV} = \sum_{t=1}^{T=8760} P_{PV,T}(t) \times ef_{PV} \times GWP \tag{20}$$

where, ef_{PV} is the emission factor of the PV system. For mono, Si PV ef_{PV} is 0.045 kgCO$_2$-eq/kWh [9, 53].

Similarly, the GHG emission from the WT system (E_{WT}) as:

$$E_{WT} = \sum_{t=1}^{T=8760} \mathrm{P}_{WT,T}(\mathrm{t}) \times ef_{WT} \times GWP \tag{21}$$

where, ef_{WT} is the emission factor of the WT system. Here, $ef_{WT} = 0.011$ kgCO$_2$-eq/kWh [54].

The GHG emission from BESS(E_{BESS}) occurs during the manufacturing and operation phase [55]. The yearly emissions are evaluated as:

$$E_{BESS} = \left(\mathrm{N}_{bat} \times \frac{C_{bat}}{L_{bat}} \times e_{BESS}^{co} + \sum_{t=1}^{T=8760} \mathrm{P}_{bd}(\mathrm{t}) \times e_{BESS}^{op} \right)$$
$$\times GWP \tag{22}$$

where, L_{bat} is the lifetime of the battery, e_{BESS}^{co} is the emission factor of the BESS for the construction phase (149 kgCO$_2$-eq/kWh) for lead acid battery [56], e_{BESS}^{op} is the emission factor of the BESS for the operation phase (0.004 kgCO$_2$-eq/kWh) [55] and P_{bd} is the power delivered by BESS.

The total GHG emissions for the proposed microgrid (GHG_{TL_MG}) and net savings in GHG emission (GHG_{Net_Svg}) are evaluated as:

$$GHG_{TL\_MG} = E_{PV} + E_{WTG} + E_{BES} \tag{23}$$

$$GHG_{Net\_Svg} = GHG_{grid} - GHG_{TL\_MG} \tag{24}$$

4 Problem Formulation

4.1 Objective Function

The objective function is to minimize the LCOE for the proposed microgrid subjected to constraints. $P_{\mathrm{Res,T}}$ is evaluated as:

$$P_{\mathrm{Res,T}}(t) = N_{PV} \times P_{PV}(t) + N_{WTG} \times P_{WTG}(t) \tag{25}$$

The LCOE is a function of the N_{PV}, N_{WTG} and N_{bat}. Thus, the objective function is given as:

$$F = \min\{LCOE(N_{PV}, N_{WTG}, N_{bat})\} \tag{26}$$

4.2 Constraints

4.2.1 Operational constraints

The operational constraints are

$$\left.\begin{array}{l} N_{PV}^{\min} \leq N_{PV} \leq N_{PV}^{\max} \\ N_{WTG}^{\min} \leq N_{WTG} \leq N_{WTG}^{\max} \\ N_{bat}^{\min} \leq N_{bat} \leq N_{bat}^{\max} \\ SOC^{\min} \leq SOC(t) \leq SOC^{\max} \end{array}\right\} \tag{27}$$

4.2.2 Reliability constraints

The reliability constraint considered is

$$LOPSP \leq LOPSP^{\max} \tag{28}$$

Here, $LOPSP^{max}$ is the maximum allowed LOPSP, which is considered 0%, 2%, and 4%.

The LOPSP is a reliability index with values between 0 and 1, and 0 indicates a fully feed load, whereas 1 indicates no load is feed. It is defined as [9, 14]:

$$LOPSP = \sum_{t=1}^{T=8760} LOPS(t) \bigg/ \sum_{t=1}^{T=8760} P_L(t) \tag{29}$$

The solutions need to satisfy the above constraint to be considered optimal.

4.3 Flowchart of Operational Strategy

Figure 3 depicts the flowchart for the proposed microgrid optimal design and energy management for the year. Set day $d = 1$ first, then calculate the hourly power using G_h and v data. The total RESs power generated, load demand, and battery SOC determine the BESS status, i.e., whether to charge or discharge the battery. Thereafter, the constraints are checked to be within the range limit. The DA, GWO, DE, and DHS algorithms are used for optimization. If the evaluations are finished for the day, they are repeated the next day until the entire year is completed.

5 Dragonfly Optimization Algorithms

DA imitates dragonfly swarming behaviour [36]. There are nearly 3000 different species of dragonflies in the world. Dragonflies swarm to pursue two
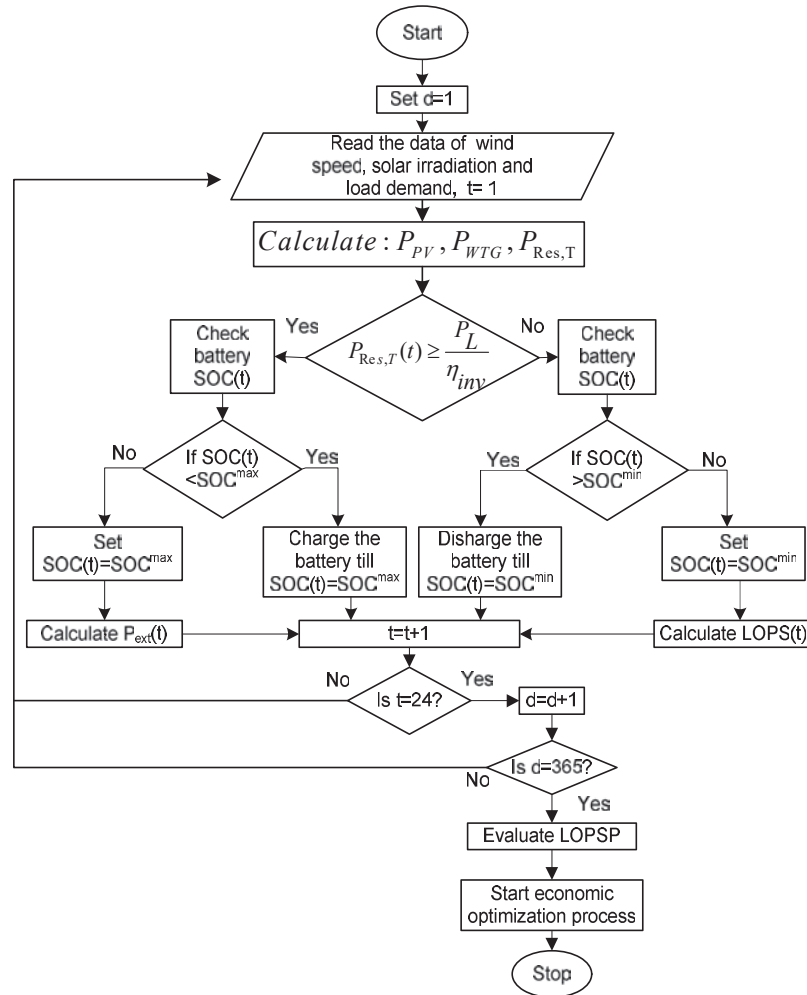
Figure 3 Flowchart of operational strategy.

objectives: hunting and migration. Static swarm refers to hunting, whereas dynamic swarm refers to migration. They form small groups and fly back and forth over a small area, hunting other flying prey such as mosquitoes and butterflies. In a dynamic swarm, massive numbers of dragonflies swarm to migrate in one direction over long distances.

Dragonfly static and dynamic swarming behaviours are similar to the two main phases of meta-heuristic optimization: exploration and exploitation.

Dragonfly static and dynamic swarming behaviours are similar to the two main phases of meta-heuristic optimization: exploration and exploitation. The swarm's main aim is survival, so all these individuals should attract toward sources and distract outward enemies. Considering these two behaviours, five main factors are used to update the position of individual swarms: separation (S_j), alignment (A_j), cohesion (C_j), attraction towards food (F_j), and distance from the enemy (Ej). These behaviours are given as [36]:

$$S_j = -\sum_{k=1}^{N} X - X_k \tag{30}$$

$$A_j = \frac{\sum_{k=1}^{N} V_k}{N} \tag{31}$$

$$C_j = \frac{\sum_{k=1}^{N} X_k}{N} - X \tag{32}$$

$$F_j = X^+ - X \tag{33}$$

$$E_j = X^- + X \tag{34}$$

where, X indicates the position of the current individual, X_k represents the position of kth neighbouring individual, V_k depicts the velocity of kth neighboring individual, N is the number of neighboring individuals, C_j is the cohesion for of jth individual, X^+ indicates the position of food source and X^- represents the position of the enemy.

The DA uses step vector ΔX and position vector X for updating the position in search space as:

$$\Delta X_{t+1} = (sS_j + aA_j + cC_j + fF_j + eE_j) + w\Delta X_t \tag{35}$$

$$X_{t+1} = X_t + \Delta X_{t+1} \tag{36}$$

where w is inertia weight, and t indicates current iteration.

The levy flight factor improves the randomness when there is no neighbouring solution. The detailed algorithm is available in [36].

The GWO algorithm in detail is discussed in [37]. The following advantages of the GWO algorithm tempt the research community to use it: (i) it requires only two parameters for initialization; (ii) it has a relatively fast convergence rate; (iii) it can be easily generalized to the next space; and (iv) it has a shorter runtime [57]. DE algorithm detailed in [38]. The DE

algorithm has the following advantages: (i) ability to handle nonlinear, non-differentiable, noise, time-dependent, and multimodal cost function, (ii) ease of use due to fewer control variables and fast rate of convergence, (iii) effective global optimization capability, (iv) applicable for discrete, integer and mixed parameter optimization etc. [58]. The DHS algorithm detailed in [5,39], has gained attention due to its simplicity, fewer parameters, and easy implementation [39].

6 Results and Discussions

The proposed microgrid primary energy sources are PV and WT, with BESS as an energy storage system. Figure 1 shows the availability of solar irradiation, wind speed and electrical load demand. The cost of components and economic parameters influences the TLCC of the microgrid. Table B2 lists the price and other information about the microgrid components. The various source configurations are considered for the study include: *Configuration-I*: PV-WT-BESS, *Configuration-II*: PV-BESS, and *Configuration-III*: WT-BESS.

   The reliability of each configuration is assessed by taking into account Case-I: $\text{LOPSP}^{\text{max}} = 0\%$, Case-II: $\text{LOPSP}^{\text{max}} = 2\%$, and Case-III: $\text{LOPSP}^{\text{max}} = 4\%$. The simulations are run on the MATLAB platform for the entire year while considering the same generated power each year until the project completion and a consistent load profile. The optimal value is considered for optimal design and energy management based on the simulation findings, which were achieved using 25 separate runs. Table B3 displays the optimization algorithms parameters. The economic parameters δ, γ, and i are 8%, 7.5% and 6% respectively, and L_p is 20 years.

6.1 Configuration-I

Table 2 shows the results for Configuration-I. As opposed to 0.1290 \$/kWh and 0.1173 \$/kWh in Case-I and Case-II, respectively, it demonstrates that the LCOE is lowest in Case-III with DA, GWO, and DE, at 0.1056 \$/kWh. With the LOPSP reliability limitation being relaxed, the LCOE falls. The values of the decision variables are always the same for DA and GWO. The optimal values of N_{PV} and N_{WTG} are 164 and 100, respectively, for all cases, with different N_{bat} using DA and GWO. In Case-III, the N_{bat} decreases, resulting in a reduced LOCE and TLCC. With the DA and GWO algorithms, the N_{bat} for Cases I, II, and III, respectively, are 2170, 1815, and 1460. In all cases,

Table 2   Results obtained for Configuration-I

Case	Algorithm	N_{PV}	N_{WTG}	N_{bat}	N_{inv}	TLCC (M\$)	LCOE (\$/kWh)	LOPSP (%)	Iteration for Convergence
I	DA	164	100	2170	60	3.450	0.1290	0.0	66
	GWO	164	100	2170	60	3.450	0.1290	0.0	159
	DE	162	100	2172	60	3.450	0.1290	0.0	95
	DHS	367	90	2330	60	3.633	0.1358	0.0	59
II	DA	164	100	1815	60	3.137	0.1173	2.0	102
	GWO	164	100	1815	60	3.137	0.1173	2.0	105
	DE	163	100	1816	60	3.137	0.1173	2.0	104
	DHS	561	98	1608	60	3.269	0.1222	1.96	56
III	DA	164	100	1460	60	2.825	0.1056	4.0	118
	GWO	164	100	1460	60	2.825	0.1056	4.0	152
	DE	164	100	1460	60	2.825	0.1056	4.0	141
	DHS	247	91	1838	60	3.110	0.1163	3.61	122

the DE gives similar LCOE and TLCC as DA and GWO algorithms, with different values of decision variables, as shown in Table 2. Compared to DA, GWO, and DE, the LCOE value generated by the DHS method is higher. DHS, however, has the fastest convergence. It shows that DHS is more likely to come up with less-than-ideal solutions when compared to DA, GWO, and DE. It also shows that at the optimal value of decision variables, the LOPSP $<$ LOPSP^{max}, and at the optimal value, DA has the fastest convergence rate, followed by DE and GWO. Figure 4 shows the convergence characteristics of the optimization algorithms. Figure 5, depicting the SOC variation of BESS for all three cases, shows that during the 9th–10th hours SOC of BESS is on the lower side after discharging from 1–10 hours, while charged from 11–20 hours and further getting discharged to meet the *PL*. The optimal generations and load patterns shown in Figure 6, show that BESS can be used to manage energy optimally while RES-based optimal generation can fulfil the P_L. Figure 6 also shows that optimal power generation by WT is sufficient at low air density which indicates its feasibility for electrical energy generation at lower air density area.

6.2 Configuration-II

The WT is unavailable in this configuration, and PV is available only, requiring more number of BESSs to meet the load demand during night hours. Table 3 presents the results for all cases. Similar to Configuration-I, Case-III has a minimum LCOE of 0.1653 \$/kWh, which is lower than 0.1710 \$/kWh
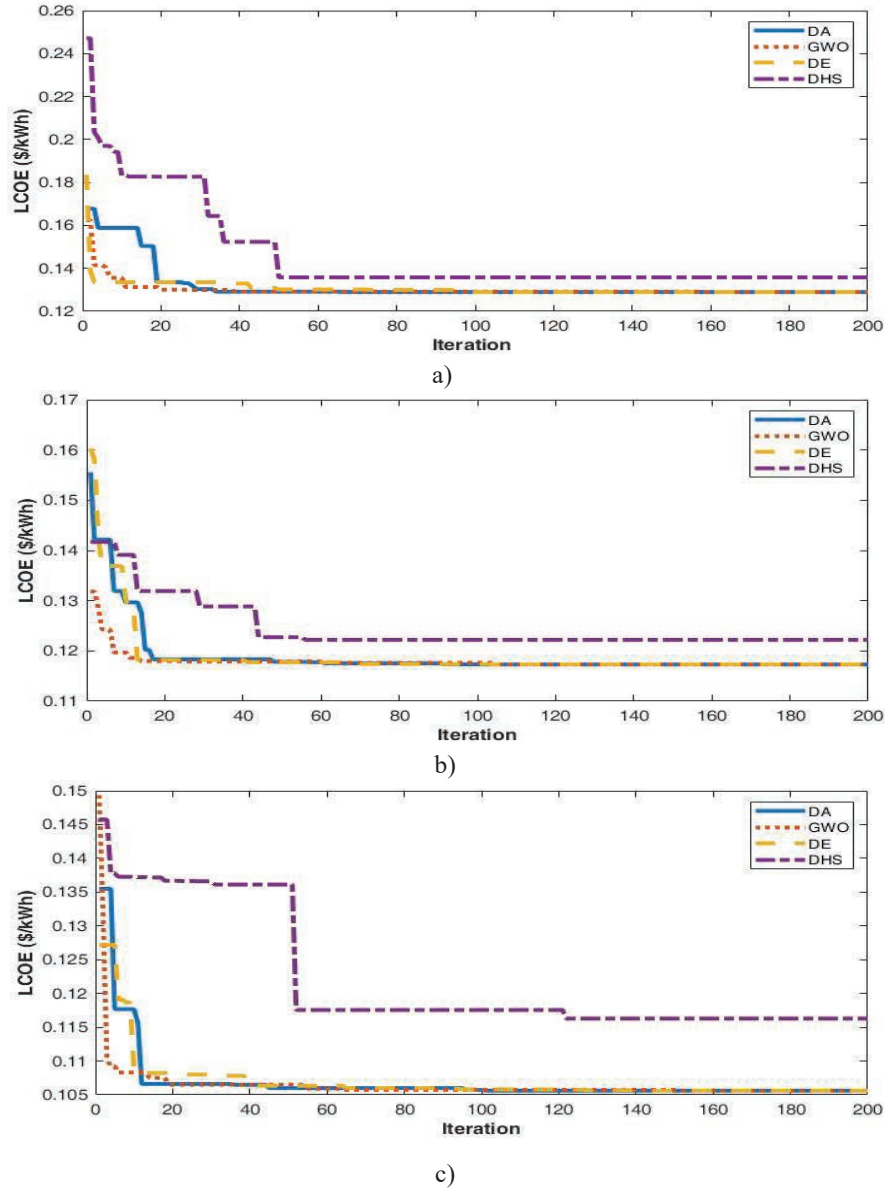
Figure 4 Convergence characteristics for the optimization algorithms used in Configuration-I, (a) Case-I, (b) Case-II, and (c) Case-III.
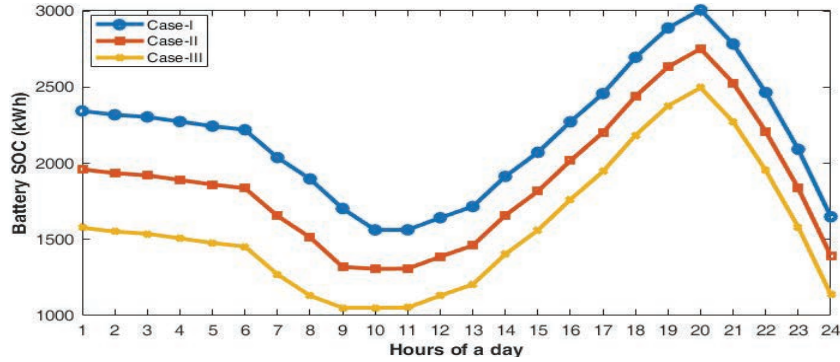
Figure 5 Variation of SOC for Configuration-I using DA.

and 0.1887 \$/kWh for Case-II and Case-I, respectively, with DA, GWO, and DE. The $N_{PV} = 1350$, and $N_{bat} = 4330$ for Case-I, and $N_{PV} = 350$, and $N_{bat} = 3975$ for Case-II, similarly $N_{PV} = 350$, and $N_{bat} = 3620$ for Case-III, with DA and GWO. Like Configuration-I, DE, and DHS have marginally different N_{PV} and N_{bat} values, but LCOE and TLCC produced from DE are identical to DA and GWO. Additionally, it should be noted that DA, DE, and GWO have the fastest convergence rates when choosing the optimum LCOE value. The LOPSP is obtained within LOPSP^{max}. The convergence characteristics of the DA, GWO, DE, and DHS algorithms are shown in Figure A1 (Appendix A). It also suggests that DHS may lead to sub-optimal solutions. The variation of BESS SOC is shown in Figure A2. It indicates that it charges during the day from 11 to 19 hours and discharges during the night from 1 to 10 and 20 to 24 hours. Figure A3 depicts the generation and load patterns. It shows that PV with BESS can meet the P_L and that BESS can help achieve effective energy management. However, the LCOE is significantly greater than that of Configuration-I due to the large number of N_{PV} and N_{bat}.

6.3 Configuration-III

The configuration only has WT and BESS to handle the load demand, which causes N_{bat} to be higher. Table 4 displays the results. The LCOE for DA, GWO, and DE is the lowest in Case-III, at 0.1586 \$/kWh compared to 0.1703 \$/kWh and 0.1819 \$/kWh in Case-II and Case-I, respectively. The optimal value of N_{WTG} is 100 in all cases, whereas N_{bat} has distinct values, 3939, 3584, and 3229 for Case-I, Case-II, and Case-III, respectively, with
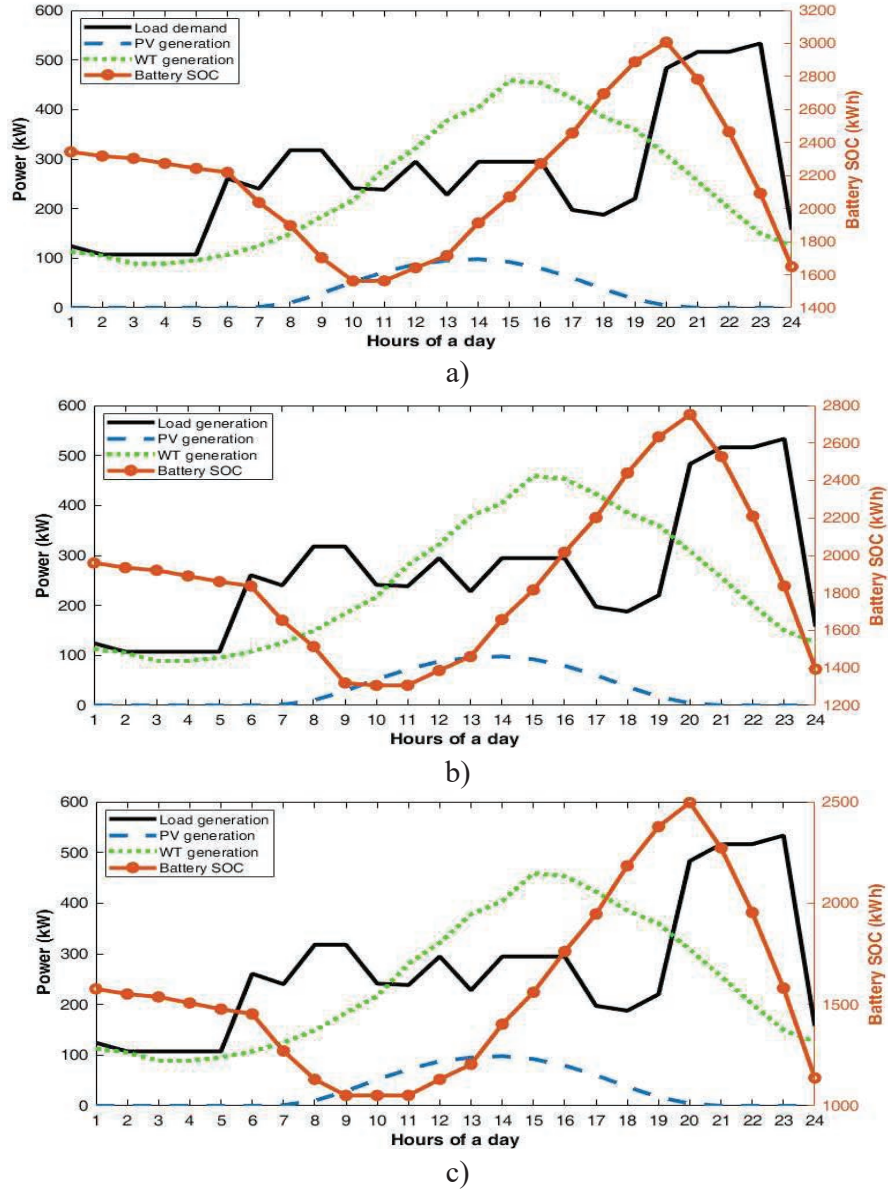
Figure 6 Generation and load profile for Configuration-I, (a) Case-I, (b) Case-II, and (c) Case-III.

Table 3   Results obtained for Configuration-II

Case	Algorithm	N_{PV}	N_{WTG}	N_{bat}	N_{inv}	TLCC (M$)	LCOE ($/kWh)	LOPSP (%)	Iteration for Convergence
I	DA	1350	–	4330	60	5.047	0.1887	0.0	100
	GWO	1350	–	4330	60	5.047	0.1887	0.0	181
	DE	1350	–	4330	60	5.047	0.1887	0.0	109
	DHS	1352	–	4382	60	5.094	0.1905	0.0	156
II	DA	1350	–	3975	60	4.734	0.1770	2.0	100
	GWO	1350	–	3975	60	4.734	0.1770	2.0	177
	DE	1349	–	3976	60	4.734	0.1770	2.0	135
	DHS	1354	–	3974	60	4.737	0.1771	1.99	71
III	DA	1350	–	3620	60	4.422	0.1653	4.0	103
	GWO	1350	–	3620	60	4.422	0.1653	4.0	160
	DE	1350	–	3620	60	4.422	0.1653	4.0	105
	DHS	1362	–	3621	60	4.433	0.1658	3.95	90

DA, GWO, and DE, similar to Configuration-I. Table 4 shows that similar to Configuration-I and -II, DA has the fastest convergence rate, followed by DE and GWO. Additionally, LOPSP is limited by LOPSP^{max} limits. Figure A4 depict the convergence of the DA, GWO, DE, and DHS algorithms, indicating that DHS may have sub-optimal solutions. Figure A5 shows the SOC fluctuation of the BESS, which shows discharge from 0 to 10 hours and charging from 13 to 20 hours before discharging to satisfy the P_L. The generation and load profile in Figure A6 demonstrates how the BESS enables meeting P_L with effective energy management. This configuration LCOE is higher than Configuration-I and lower than Configuration-II. As a result, Configuration-I has the lowest LCOE. Figure A6 also shows that optimal power generation by only WT is sufficient to meet the P_L with the BESS combination, confirming its feasibility at low air density sites.

6.4 Statistical Analysis

The results above demonstrate that DA offers superior results over GWO, DE, and DHS. Statistical analysis has confirmed the effectiveness of DA, GWO, DE, and DHS in minimizing the LCOE and managing energy. However, DHS provides a comparatively higher value of LOCE. The DA, GWO, and DE also offer similar decision factors values. Each algorithm undergoes 25 independent runs, with recording the LCOE. The values of LCOE's maximum, minimum, mean, median, and standard deviation are shown in

Table 4 Results obtained for Configuration-III

Case	Algorithm	N_{PV}	N_{WTG}	N_{bat}	N_{inv}	TLCC (M\$)	LCOE (\$/kWh)	LOPSP (%)	Iteration for Convergence
I	DA	–	100	3939	60	4.866	0.1819	0.0	12
	GWO	–	100	3939	60	4.866	0.1819	0.0	45
	DE	–	100	3939	60	4.866	0.1819	0.0	27
	DHS	–	98	4274	60	5.134	0.1920	0.0	111
II	DA	–	100	3584	60	4.554	0.1703	2.0	7
	GWO	–	100	3584	60	4.554	0.1703	2.0	50
	DE	–	100	3584	60	4.554	0.1703	2.0	19
	DHS	–	98	3942	60	4.842	0.1811	1.69	38
III	DA	–	100	3229	60	4.241	0.1586	4.0	15
	GWO	–	100	3229	60	4.241	0.1586	4.0	27
	DE	–	100	3229	60	4.241	0.1586	4.0	25
	DHS	–	100	3257	60	4.266	0.1595	3.84	16

Table B4. Comparing DA to GWO, DE, and DHS, it is evident that DA has a lower standard deviation across all configurations. It can also be shown from Tables 2, 3, and 4 that DA has the fastest rate of convergence and needs the least iterations to achieve convergence, followed by DE and GWO. Therefore, DA is best in such applications with reliability, accuracy, and convergence rate.

6.5 Sensitivity Analysis

Figure 7(a) and 7(b) illustrate the variation of LCOE and TLCC with LOPSP^{max}, respectively. Figure 7(a) demonstrates that the LCOE for a reliable source is high and declines with declining system reliability, whereas Figure 7(b) demonstrates that the TLCC is larger for highly reliable systems and declines as the reliability index LOPSP^{max} increases.

6.6 GHG Emission Analysis

Table 5 displays the GHG emission of the optimal microgrid (Configuration-I, Case-I). It covers the weight of emissions for CO_2, CH_4, N_2O, and SF_6. The table also shows the proposed microgrid's net reduction in GHG emissions compared to the base case. It is assumed that the entire load is met by the grid supplied in the base case. The total GHG emissions resulting from the base scenario, PV, and WT are 74577372.48 tons, 293449.52 tons,
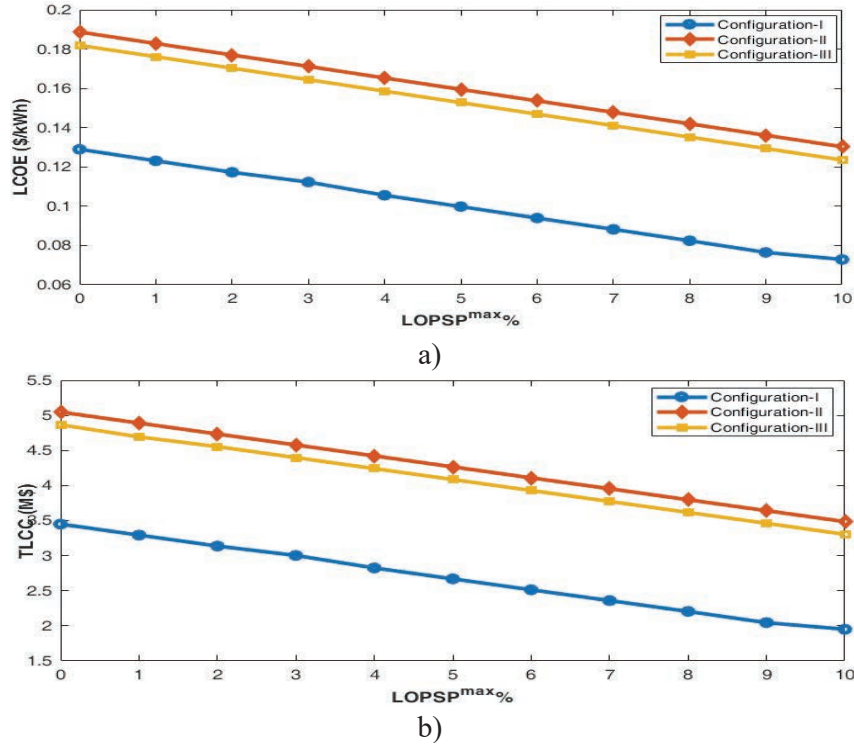
a)

b)

Figure 7 Variations of (a) LCOE and (b) TLCC versus LOPSP^{max}% for DA.

Table 5 The annual GHG emission from Configuration-I microgrid

Case	GHG Emission Types	Base Case (Tons)	PV (Tons)	WT (Tons)	BESS (Tons)	Net Saving (Tons)
I	CO_2	3077.64	12.11	23.2	235.99	2806.34
	CH_4	64630.44	254.31	487.2	4955.79	58933.14
	N_2O	954068.40	3754.1	7192	73156.9	869965.4
	SF_6	73555596.00	289429	554480	5640161	67071526
	Total GHG emission	74577372.48	293449.52	562182.4	5718509.7	68003230.9

and 562182.4 tons, respectively. Optimal microgrid Configuration-I, Case-I reduce GHG emissions by 91.2% compared to a base case. Figure 8 shows the cumulative annual CO_2 emissions from Configuration-I, Configuration-II, and Configuration-III. Additionally, it shows that, as a result of having more N_{bat}, Configuration-II has the most CO_2 emissions, followed by Configuration-III, and Configuration-I has the lowest. The CO_2 emission
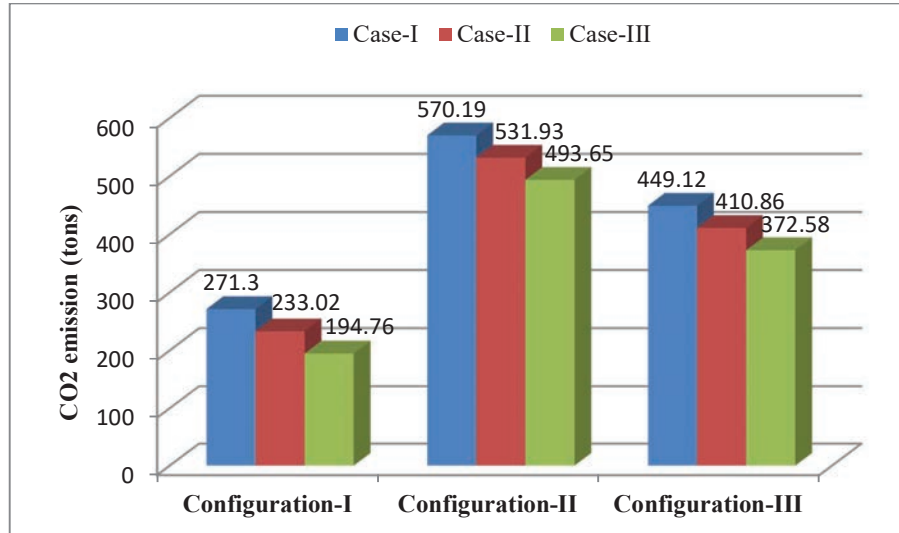
Figure 8 Total annual CO_2 emission from proposed microgrids.

in Case-III for all configurations, shown in Figure 8, is lowest due to using least generating and BESS units with maximum relaxation of 4% in $LOPSP^{max}$. According to the aforementioned findings, Configuration-I has the lowest LCOE and CO_2 emission rates. Therefore, Configuration-I is deemed appropriate from an environmental and an economic perspective.

Thus, from the analysis it is evident that the electricity supplied to the site under consideration by the proposed PV/WT/BESS based isolated microgrid is clean and environmental friendly. This proposed microgird has the ability to mitigate the adverse environmental impacts possessed by a conventional power plant in terms of climate change, global warming, human health, acid rain, air pollution, and photochemical smog etc. This study will have potential role for power supply to the local residents of remote hilly areas like Leh and Ladhakh, Lahul and Spiti in Himachal Pradesh, India. The proposed micro-grid has promising role in making the life of local residents comfortable in harsh environment. Further, the degradable aspects like deforestation done in such hilly areas for wood as a fuel source in winter will save the environment. Moreover, this study will help in saving the environment by reducing the natural calamities like cloud burst. The degradable impacts of cloud burst on the local residents will be minimized due less erosion of soil and also due to better ecological balance. Overall, it is apt to state that, with the proposal of

Table 6   Different configurations of previous studies and the proposed plan

System Configuration	Operation Mode	Location	Study Year	TNPC/ TLCC (M$)	COE ($/kWh)	Ref.
PV/WT/BESS	Isolated	India	–	3.450	0.129	Current Study
PV/WT/Biomass/ BESS	Isolated	Saudi Arabia	2020	0.581	0.254	[9]
PV/WT/BESS	Isolated	Jeju Island, Korea	2020	84300	0.420	[16]
PV/WT/BESS/FC	Isolated	South Africa	2022	0.009	0.701	[17]
PV/WT/DG/BESS	Isolated	India	2022	0.233	0.183	[21]
PV/WT/BESS	Isolated	Algeria	2022	0.144	0.474	[23]
PV/CSP/WT/ BESS/TES	Isolated	Oujda, Morocco	2021	913.7	0.183	[24]
PV/WT/FC	Isolated	Suez Gulf, Egypt	2021	10.437	0.429	[25]
PV/WT/Biomass/ BESS	Isolated	Fars province, Iran	2020	1.085	0.154	[26]
PV/WT/DG/BESS	Isolated	Konya, Turkey	2020	0.131	0.247	[27]
PV/WT/FC	Isolated	Beni-Suef, Egypt	2020	2.698	0.450	[28]
PV/WT/BESS	Isolated	South Australia	2021	0.034	0.570	[29]
PV/WT/BESS/ Biomass	Isolated	China	2023	6.701	0.273	[30]
PV/WT/Biomass/ BESS	Isolated	Patiala, India	2016	0.063	0.173	[43]
PV/WT/DG/BESS	Isolated	Rabat, Morocco	2021	0.024	0.177	[50]
PV/WT/BESS	Isolated	Iran	2022	0.626	0.233	[59]
PV/WT/DG/ /BESS	Isolated	Saudi Arabia	2022	0.465	0.354	[60]
PV/WT/BESS	Isolated	Hohhot, China	2013	1.998	0.208	[61]
PV/Biogas/BESS	Isolated	Sierra Leone	2023	0.472	0.376	[62]

the PV/WT/BESS based isolated microgrid under consideration in this study will be will be highly beneficial in such domestic hilly terrains.

6.7 Comparative Analysis

The results of the proposed microgrid are compared to microgrids existing in the literature to show their effectiveness. The comparison is shown in Table 6. The TNPC/TLCC is different due to different configurations, element sizing, and economic considerations such as capital cost, operation-maintenance cost, replacement cost, salvage value, interest, inflation, and escalation rate. Nevertheless, LCOE is the essential comparative parameter to compare the

energy cost generated from RES. The previous studies have LCOE in the 0.154 to 0.701 $/kWh range. For the current study, LCOEs are 0.1290 $/kWh, 0.1173 $/kWh, and 0.1056 $/kWh for 0%, 2%, and 4% of LOPSP^{max} respectively, which is the lowest LCOE compared to previous studies.

7 Conclusions

This paper proposes an optimal microgrid design for the village hamlet in Leh and Ladakh, India. Using DA, GWO, DE, and DHS algorithms, the optimal number of PV, WT, and BESS is determined, considering the reliability index LOPSP. Three studies are conducted with different sources and distinct values of LOPSP^{max}. The major conclusions are

- Optimal sizing of PV, WT, and BESS are performed to minimize the LCOE through DA, GWO, DE, and DHS. DHS provides a comparatively higher value of LCOE compare to remaining three algorithms to minimize the LCOE. The statistical analysis verifies that DA offers the best compromise between robustness, accuracy, and convergence rate.
- The microgrid Configuration-I (PV/WT/BESS) provides energy at the lowest rate compared to Configuration-II (PV/BESS) and Configuration-III (WT/BESS). The LCOE from Configuration-I, Case-I is 0.129 $/kWh which is within the range of LCOE obtained in previous studies available in the literature.
- The GHG emissions are also reduced by 91.2% from Configuration-I Case-I compared to the base case supply. The emission is due to the equipment lifecycle.
- Reliability index LOPSP is used for optimal sizing of RES and BESS, ensuring supply reliability and energy management.
- LCOE and TLCC increase with rising overall system reliability by decreasing reliability constraints LOPSP^{max} towards 0. This study also confirms the feasibility of wind energy generation at low air density sites.
- Microgrid Configuration-I has the lowest LCOE and least CO_2 emission. Therefore, it is the most suitable choice for economic and environmental concerns.

The study carried out in the paper is vital for network planning and management in the far-flung rural/desert areas to meet the load requirements with hybrid energy sources available where the transporting energy from the grid is costly.
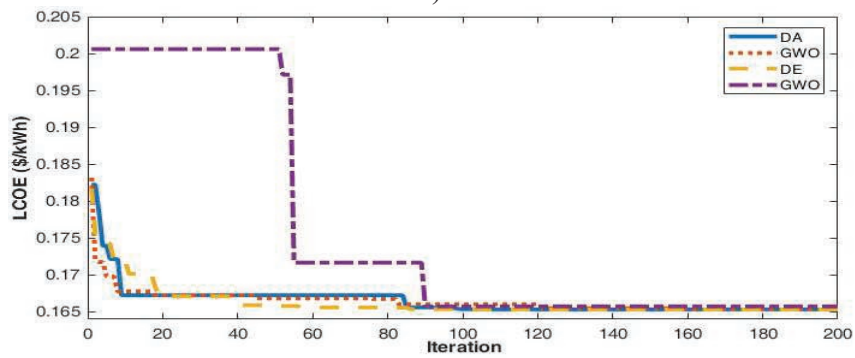
Appendix-A
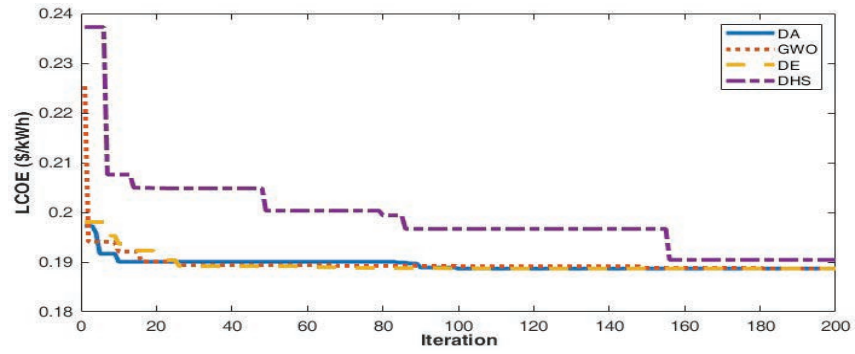
a)
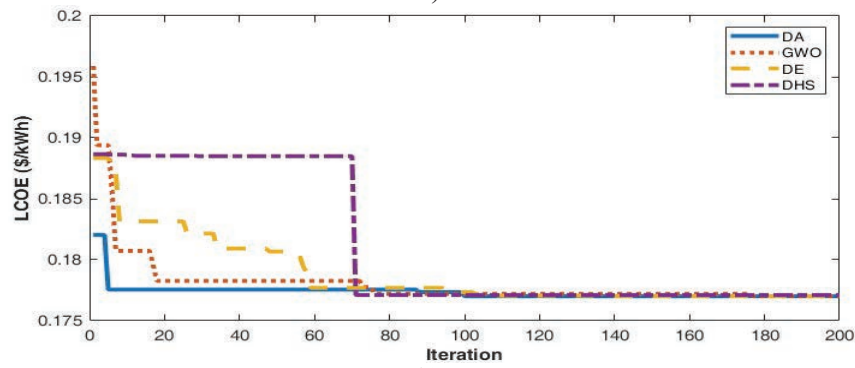
b)

c)

Figure A1 Convergence characteristics for the optimization algorithms used in Configuration-II, (a) Case-I, (b) Case-II, and (c) Case-III.
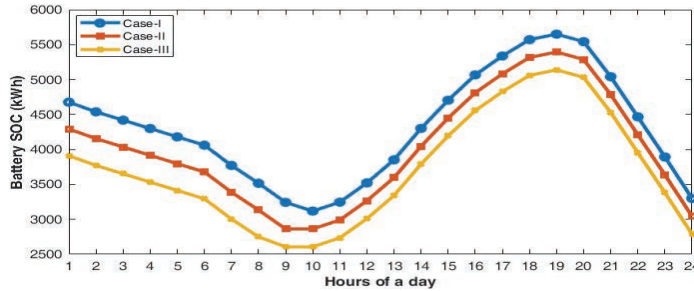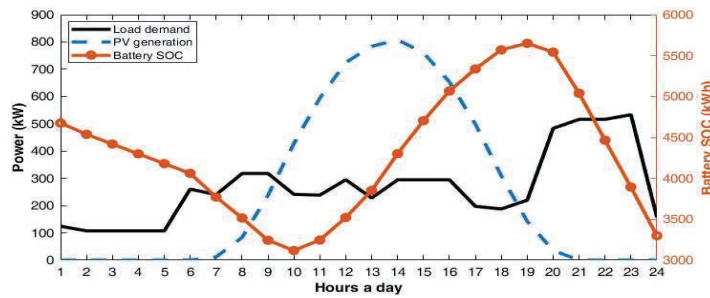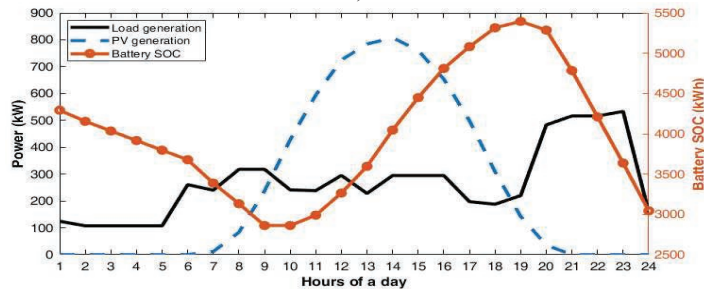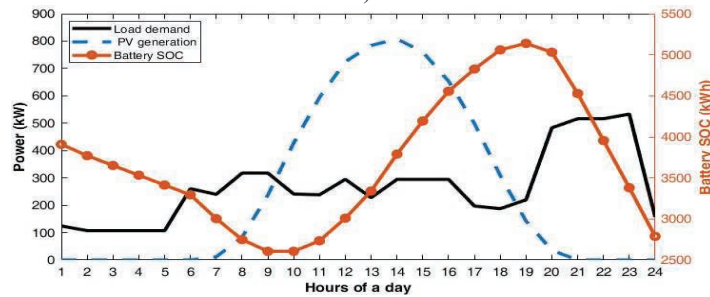
Figure A2   Variation of SOC for Configuration-II using DA.
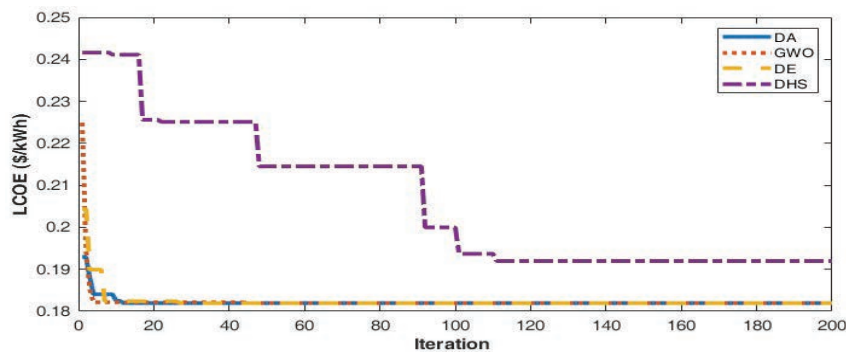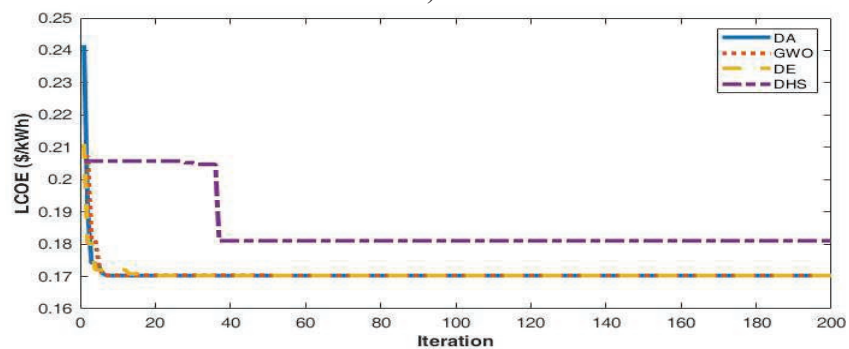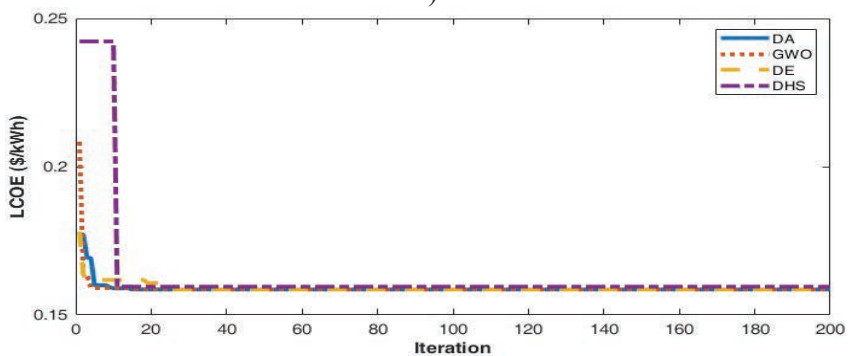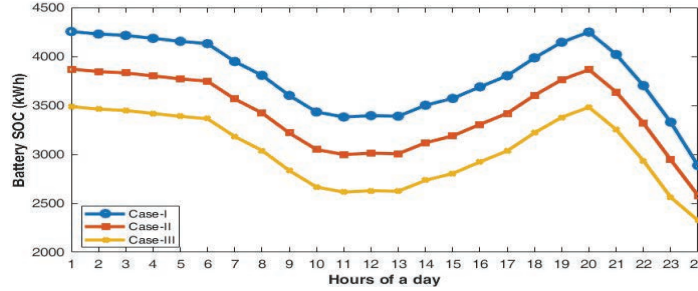

a)

b)

c)

Figure A3   Generation and load profile for Configuration-II, (a) Case-I, (b) Case-II, and (c) Case-III.

a)

b)

c)

Figure A4 Convergence characteristics for the optimization algorithms used in Configuration-III, (a) Case-I, (b) Case-II, and (c) Case-III.
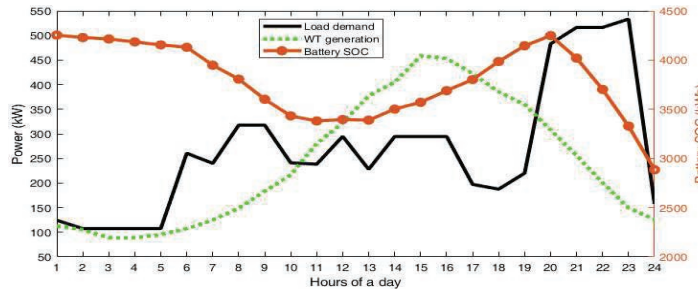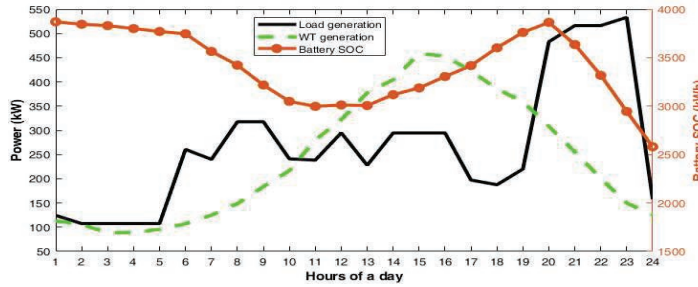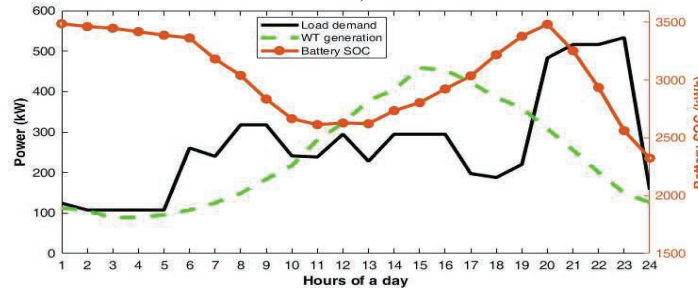
Figure A5   Variation of SOC for configuration-III using DA.

a)

b)

c)

Figure A6   Generation and load profile for Configuration-III, (a) Case-I, (b) Case-II, and (c) Case-III.

Appendix-B

Table B1   Technical parameters of microgrid components

Component	Parameters	Value	Component	Parameters	Value
Solar photovoltaic	Model type	SHARP polycrystalline	**BESS**	Battery Type	Deep cycle Lead-acid
	Rating of PV panel (P_{PV}^r)	1 kW		Nominal capacity (C_{bat})	150 Ah
	Loss factor (d_{Loss})	88%		Nominal voltage (V_n)	24 V
	Standard irradiation (G_{STC})	1 kW/m^2		Initial hour state of charge (SOC_p)	100%
Wind turbine	Model type	AEOLOS-Horizontal axis		Depth of discharge (DOD)	80%
	Rated power output (P_{RW})	10 kW		Hourly self-discharge rate (λ)	0.0
	Swept area blade (A_{Tb})	50.24 m^2		Charging efficiency (η_{bcg})	100%
	Generator efficiency (η_{WTG})	85%		Discharging efficiency (η_{bdg})	90%
	Air density (δ_{ar})	0.7 Kg/m^3	**Inverter**	Model type	Luminous NXI-310
	Power coefficient (C_P)	0.59			
	Cut-in wind speed (v_{Cin})	2.5 m/s		Rated Capacity (P_{inv}^R)	10 kW
	Rated wind speed (v_{Rt})	10 m/s			
	Cut-off wind speed (v_{Cof})	25 m/s		Efficiency (η_{inv})	90%

Table B2   Cost fraction details of microgrid components

Components	Capital Cost ($/Unit)	Operation and Maintenance Cost ($/Unit-Year)	Replacement Cost ($/Unit)	Resale Price ($/Unit)	Lifetime (Year)
Solar PV (1 kW)	1200	4	1200	300	20
Wind Turbine (10 kW)	23000	10	23000	6900	20
Battery (150 Ah)	200	2	200	20	5
Inverter (10 kW)	1270	10	1270	127	20

Table B3   Parameters for the algorithm used

DA		GWO		DE		DHS	
Technical Parameter	Value	Technical Parameter	Value	Technical Parameter	Value	Technical Parameter	Value
Maximum no. of iteration	200	Maximum no. of iteration	200	Maximum no. of iteration	200	Maximum no. of iteration	200
Search agent	50	Search agent	50	Population size	50	Harmony memory size	5.0
No. of dragonflies	10	Convergence constant (a)	[2 0]	Scaling factor lower bound	0.2–0.8	Harmony memory considering rate	0.9
Separation factor (S)	0.1	Random no. (r1)	[0 1]	Scaling factor upper bound	0.8	Pitch adjusting rate	0.1
Alignment (A)	0.1	Random no. (r2)	[0 1]	Crossover frequency	0.2	Pitch adjustment rate (Maximum)	1.0
Cohesion (C)	0.7					Pitch adjustment rate (Minimum)	0.1
Food factor (F)	1.0					Maximum value of bandwidth	1.0
Enemy factor (E)	1.0					Minimum value of bandwidth	0.1
Inertia weight (w)	0.9-0.2						

Table B4   LCOE statistics of the result from the DA, GWO, DE, and DHS

	Parameter	DA	GWO	DE	DHS
Configuration-I, Case-I	Max. ($/kWh)	0.1290	0.1290	0.1293	0.1832
	Min. ($/kWh)	0.1290	0.1290	0.1290	0.1358
	Mean ($/kWh)	0.1290	0.1290	0.1290	0.1525
	Median ($/kWh)	0.1290	0.1290	0.1290	0.1504
	STD.	8.14E-06	1.54E-05	7.84E-05	1.24E-02
Configuration-II, Case-I	Max. ($/kWh)	0.1887	0.1888	0.1895	0.2424
	Min. ($/kWh)	0.1887	0.1887	0.1887	0.1905
	Mean ($/kWh)	0.1887	0.1887	0.1888	0.2009
	Median ($/kWh)	0.1887	0.1887	0.1887	0.1948
	STD.	8.498E-17	3.15E-05	2.188E-04	1.592E-02
Configuration-III, Case-I	Max. ($/kWh)	0.1819	0.1819	0.1828	0.2385
	Min. ($/kWh)	0.1819	0.1819	0.1819	0.1920
	Mean ($/kWh)	0.1819	0.1819	0.1822	0.2110
	Median ($/kWh)	0.1819	0.1819	0.1820	0.2094
	STD.	2.833E-17	2.83E-17	2.79E-04	1.363E-02

References

[1] R. D. Daniel Schnitzer, Deepa Shinde Lounsbury, Juan Pablo Carvallo and D. M. K. Jay Apt. Microgrids for Rural Electrification: A critical review of best practices based on seven case studies. *United Nations Found.* 1–122, 2014.

[2] K. Kusakana. Techno-economic analysis of off-grid hydrokinetic-based hybrid energy systems for onshore/remote area in South Africa. *Energy*, 68:947–957, 2014. https://doi:10.1016/j.energy.2014.01.100.

[3] P. Paliwal, N. P. Patidar, and R. K. Nema. Determination of reliability constrained optimal resource mix for an autonomous hybrid power system using Particle Swarm Optimization. *Renew. Energy*, 63:194–204, 2014. https://doi:10.1016/j.renene.2013.09.003.

[4] M. S. Ismail, M. Moghavvemi, and T. M. I. Mahlia. Genetic algorithm based optimization on modeling and design of hybrid renewable energy systems. *Energy Convers. Manag.*, 85:120–130, 2014. https://doi:10.1016/j.enconman.2014.05.064.

[5] A. Chauhan and R. P. Saini. Techno-economic optimization based approach for energy management of a stand-alone integrated renewable energy system for remote areas of India. *Energy*, 94:138–156, 2016. https://doi:10.1016/j.energy.2015.10.136.

[6] A. Sunil and D. M. Venkaiah, Chintham, Vinod Kumar. Optimal Power Dispatch of Multiple DGs Using a Hybrid Algorithm for Mitigating Voltage Deviations and Losses in a Radial Distribution System with Economic Benefits. *Distrib. Gener. Altern. Energy J.*, 38(5):1531–1558, 2023. https://doi.org/10.13052/dgaej2156-3306.3858.

[7] P. Kumar, V. Das, A. K. Singh, and P. Karuppanan. Levelized Cost of Energy-Based Economic Analysis of Microgrid Equipped with Multi Energy Storage System. *Distrib. Gener. Altern. Energy J.*, 38(4):1331–1356, 2023. https://doi.org/10.13052/dgaej2156-3306.38411.

[8] K. Anoune, M. Ghazi, M. Boyua, A. Laknizi, M. Ghazouani, A.B. Abdellah and A. Astito. Optimization and techno-economic analysis of photovoltaic-wind-battery based hybrid system. *J. Energy Storage*, 32:101878, 2020. https://doi:10.1016/j.est.2020.101878.

[9] N. Alshammari and J. Asumadu. Optimum unit sizing of hybrid renewable energy system utilizing harmony search, Jaya and particle swarm optimization algorithms. *Sustain. Cities Soc.*, 60:102255, 2020. https://doi:10.1016/j.scs.2020.102255.

[10] B. A. Bhayo, H. H. Al-Kayiem, S. I. U. Gilani, and F. B. Ismail. Power management optimization of hybrid solar photovoltaic-battery integrated with pumped-hydro-storage system for standalone electricity generation. *Energy Convers. Manag.*, 215:112942, 2020. https://doi:10.1016/j.enconman.2020.112942.

[11] Y. He, S. Guo, J. Zhou, F. Wu, J. Huang, and H. Pei. The quantitative techno-economic comparisons and multi-objective capacity optimization of wind-photovoltaic hybrid power system considering different energy storage technologies. *Energy Convers. Manag.*, 229: 113779, 2021. https://doi:10.1016/j.enconman.2020.113779.

[12] N. S. Attemene, K. S. Agbli, S. Fofana, and D. Hissel. Optimal sizing of a wind, fuel cell, electrolyzer, battery and supercapacitor system for off-grid applications. *Int. J. Hydrogen Energy*, 45(8):5512–5525, 2020. https://doi:10.1016/j.ijhydene.2019.05.212.

[13] M. M. Samy, M. I. Mosaad, and S. Barakat. Optimal economic study of hybrid PV-wind-fuel cell system integrated to unreliable electric utility using hybrid search optimization technique. *Int. J. Hydrogen Energy*,46(20):11217–11231, 2021. https://doi:10.1016/j.ijhydene.2 020.07.258.

[14] S. Barakat, H. Ibrahim, and A. A. Elbaset. Multi-objective optimization of grid-connected PV-wind hybrid system considering reliability, cost, and environmental aspects. *Sustain. Cities Soc.*, 60:102178, 2020. https://doi:10.1016/j.scs.2020.102178.

[15] D. Temene, N. Donatien, T. Konchou, F. Armel, and T. Ren. Techno-economic and environmental feasibility study with demand-side management of photovoltaic/wind/hydroelectricity/Battery/ diesel:A case study in Sub-Saharan Africa. *Energy Convers. Manag.*, 258:115494, 2022. https://doi:10.1016/j.enconman.2022.115494.

[16] W. Jung, J. Jeong, J. Kim, and D. Chang. Optimization of hybrid off-grid system consisting of renewables and Li-ion batteries. *J. Power Sources*, 451:227754, 2020. https://doi:10.1016/j.jpowsour.2020.227754.

[17] O. M. Babatunde, J. L. Munda, and Y. Hamam. Off-grid hybrid photovoltaic – micro wind turbine renewable energy system with hydrogen and battery storage: Effects of sun tracking technologies. *Energy Convers. Manag.*, 255:115335, 2022.

[18] N. Ghorbani, A. Kasaeian, A. Toopshekan, L. Bahrami, and A. Maghami. Optimizing a hybrid wind-PV-battery system using GA-PSO and MOPSO for reducing cost and increasing reliability. *Energy*,154:581–591, 2018. https://doi:10.1016/j.energy.2017.12.057.

[19] M. S. Javed, T. Ma, J. Jurasz, S. Ahmed, and J. Mikulik. Performance comparison of heuristic algorithms for optimization of hybrid off-grid renewable energy systems. *Energy*, 210:118599, 2020. https://doi:10.1 016/j.energy.2020.118599.

[20] M. Najafi Ashtiani, A. Toopshekan, F. Razi Astaraei, H. Yousefi, and A. Maleki. Techno-economic analysis of a grid-connected PV/battery system using the teaching-learning-based optimization algorithm. *Sol. Energy*, 203:69–82, 2020. https://doi:10.1016/j.solener.2020.04.007.

[21] F. A. Khan, N. Pal, S. H. Saeed, and A. Yadav. Techno-economic and feasibility assessment of standalone solar Photovoltaic/Wind hybrid energy system for various storage techniques and different rural locations in India. *Energy Convers. Manag.*, 270: 116217, 2022. https://doi: 10.1016/j.enconman.2022.116217.

[22] M. Jahannoosh, S. A. Nowdeh, A. Naderipour, H. Kamyab, I. F. Davoudkhani, and J. J. Klemeš. New hybrid meta-heuristic algorithm for reliable and cost-effective designing of photovoltaic/wind/fuel cell energy system considering load interruption probability. *J. Clean. Prod.*, 278:123406, 2021. https://doi:10.1016/j.jclepro.2020.123406.

[23] D. Fares, M. Fathi, and S. Mekhilef. Performance evaluation of metaheuristic techniques for optimal sizing of a stand-alone hybrid PV/wind/battery system. *Appl. Energy*, 305: 117823, 2022. https://doi: 10.1016/j.apenergy.2021.117823.

[24] M. Chennaif, H. Zahboune, M. Elhafyani, and S. Zouggar. Electric System Cascade Extended Analysis for optimal sizing of an autonomous hybrid CSP/PV/wind system with Battery Energy Storage System and thermal energy storage. *Energy*, 227:120444, 2021. https://doi:10.1016/ j.energy.2021.120444.

[25] H. M. Sultan, A. S. Menesy, S. Kamel, A. Korashy, S. A. Almohaimeed, and M. Abdel-akher. An improved artificial ecosystem optimization algorithm for optimal configuration of a hybrid PV / WT / FC energy system. *Alexandria Eng. J.*, 60:1001–1025, 2021. https://doi:10.1016/j. aej.2020.10.027.

[26] M. H. Jahangir and R. Cheraghi. Economic and environmental assessment of solar-wind-biomass hybrid renewable energy system supplying rural settlement load. *Sustain. Energy Technol. Assessments*, 42:100895,2020. https://doi:10.1016/j.seta.2020.100895.

[27] A. F. Altun and M. Kilic. Design and performance evaluation based on economics and environmental impact of a PV-wind-diesel and battery

standalone power system for various climates in Turkey. *Renew. Energy*, vol. 157:424–443, 2020. https://doi:10.1016/j.renene.2020.05.042.

[28] M. M. Samy, S. Barakat, and H. S. Ramadan. Techno-economic analysis for rustic electrification in Egypt using multi-source renewable energy based on PV/ wind/ FC. *Int. J. Hydrogen Energy*, 45(20):11471–11483, 2020. https://doi:10.1016/j.ijhydene.2019.04.038.

[29] R. Khezri, A. Mahmoudi, and H. Mohammed. A Demand Side Management Approach for Optimal Sizing of Standalone Renewable-Battery Systems. *IEEE Trans. Sustain. Energy*, 12(4):2184–2194, 2021. https://doi:10.1109/TSTE.2021.3084245.

[30] X. Xu, Z. Zhang, J. Yuan, and J. Shao. Design and multi-objective comprehensive evaluation analysis of PV-WT-BG-Battery hybrid renewable energy systems in urban communities. *Energy Convers. Manag.*, 18:100357, 2023.

[31] G. Fosso, P. Tiam, F. Lenine, and D. Koffi. Techno-economic investigation of an environmentally friendly small-scale solar tracker-based PV/wind/Battery hybrid system for off-grid rural electrification in the mount bamboutos, Cameroon. *Energy Strateg. Rev.*, 48:101107, 2023. https://doi.org/10.1016/j.esr.2023.101107.

[32] J. Kumagai. Lights for the enlightened. *IEEE Spectr.*, 53(12):32–39, 2016.

[33] N. J. Williams, P. Jaramillo, J. Taneja, and T. S. Ustun. Enabling private sector investment in microgrid-based rural electrification in developing countries: A review. *Renew. Sustain. Energy Rev.*,52:1268–1281, 2015. https://doi:10.1016/j.rser.2015.07.153.

[34] P. K. Sharma, S. Ahmed, and V. Warudkar. A preliminary study of wind–solar hybrid systems potential in Jammu and Kashmir. *Int. J. Ambient Energy*, 41(9):1026–1030, 2020. https://doi:10.1080/01430750.2018.15 01743.

[35] A. report On Wind/Solar Resource Assessment studies in Leh-Ladakh UT 6. 2019.

[36] S. Mirjalili. Dragonfly algorithm: a new meta-heuristic optimization technique for solving single-objective, discrete, and multi-objective problems. *Neural Comput. Appl.*, 27(4): 1053–1073, 2016. https://doi:10.1007/s00521-015-1920-1.

[37] S. Mirjalili, S. M. Mirjalili, and A. Lewis. Grey Wolf Optimizer. *Adv. Eng. Softw.*, 69:46–61, 2014. https://doi:10.1016/j.advengsoft.2013.12.007.

[38] R. Storn and K. Price. Differential Evolution - A Simple and Efficient Heuristic for Global Optimization over Continuous Spaces. *J. Glob. Optim.*, 11(4):341–359, 1997. https://doi:10.1023/A:1008202821328.

[39] A. Askarzadeh. A discrete chaotic harmony search-based simulated annealing algorithm for optimum design of PV / wind hybrid system. *Sol. Energy*, 97:93–101, 2013. https://doi:10.1016/j.solener.20 13.08.014.

[40] A. G. Hussien, M. Amin, M. Wang, G. Liang, A. Alsanad, A. Gumaei and H. Chen. Crow Search Algorithm: Theory, Recent Advances, and Applications. *IEEE Access*, 8:173548, 2020. https://doi:10.1109/ACCE SS.2020.3024108.

[41] J. & K. Census of India 2011. District census handbook Leh 2011. 2011.

[42] A. Askarzadeh and A. Rezazadeh. Parameter identification for solar cell models using harmony search-based algorithms. *Sol. Energy*, 86: 3241–3249, 2012. https://doi:0.1016/j.solener.2012.08.018.

[43] S. Singh, M. Singh, and S. C. Kaushik. Feasibility study of an islanded microgrid in rural area consisting of PV, wind, biomass and battery energy storage system. *Energy Convers. Manag.*, 128:178–190, 2016. https://doi:10.1016/j.enconman.2016.09.046.

[44] A. Askarzadeh and L. dos Santos Coelho. A novel framework for optimization of a grid independent hybrid renewable energy system: A case study of Iran. *Sol. Energy*,112:383–396, 2015. https://doi: 10.1016/j.solener.2014.12.013.

[45] Yong Yang and Rong Li. Techno-Economic Optimization of an Off-Grid Solar/Wind/Battery Hybrid System with a Novel Multi-Objective Differential Evolution Algorithm. *Energies*, 13:1–16, 2020. https://doi: 10.3390/en13071585.

[46] A. Kashefi Kaviani, G. H. Riahy, and S. M. Kouhsari. Optimal design of a reliable hydrogen-based stand-alone wind/PV generating system, considering component outages. *Renew. Energy*, 34(11):2380–2390, 2009. https://doi:10.1016/j.renene.2009.03.020.

[47] H. Jinglin, H. Ping, Z. Hui, H. Chunguang, R. Hou, and L. Bo. Multi-objective Collaborative Planning Method for Micro-energy Systems Considering Thermoelectric Coupling Clusters. *Distrib. Gener. Altern. Energy J.*, 38(5):1677–1706, 2023. https://doi:10.13052/dgaej2156-330 6.38514.

[48] Y. P. Xu, P. Ouyang, S. M. Xing, L. Y. Qi, M. khayatnezhad, and H. Jafari. Optimal structure design of a PV/FC HRES using amended Water Strider Algorithm. *Energy Reports*,7:2057–2067, 2021.

[49] A. Maleki and A. Askarzadeh. Optimal sizing of a PV/wind/diesel system with battery storage for electrification to an off-grid remote region: A case study of Rafsanjan, Iran. *Sustain. Energy Technol. Assessments*,7:147–153, 2014. https://doi:10.1016/j.eta.2014.04.005.

[50] M. Kharrich, O. H. Mohammed, N. Alshammari, and M. Akherraz. Multi-objective optimization and the effect of the economic factors on the design of the microgrid hybrid system. *Sustain. Cities Soc.*, 65:102646, 2021. https://doi:10.1016/j.scs.2020.102646.

[51] Gunnar Myhre and Drew Shindell. *Anthropogenic and Natural Radiative Forcing*. 2014.

[52] M. Brander, A. Sood, C. Wylie, A. Haughton, J. Lovell. Electricity-specific emission factors for electricity. *Ecometrica*, 1–22, 2011.

[53] M. Brander, A. Sood, C. Wylie, A. Haughton, and J. Lovell. Electricity-specific emission factors for electricity. *Ecometrica*, 1–22, 2011.

[54] J. Peng, L. Lu, and H. Yang. Review on life cycle assessment of energy payback and greenhouse gas emission of solar photovoltaic systems. *Renew. Sustain. Energy Rev.*, 19:255–274, 2013. https://doi:10.1016/j.rser.2012.11.035.

[55] T. Ackermann. Distributed generation: a definition. *Electr. Power Syst. Res.*, 57:195–204, 2001.

[56] P. Denholm and G. L. Kulcinski. Life cycle energy requirements and greenhouse gas emissions from large scale energy storage systems. *Energy Convers. Manag.*,45(13): 2153–2172, 2004. https://doi:10.1016/j.enconman.2003.10.014.

[57] C. Mostert, B. Ostrander, S. Bringezu, and T. M. Kneiske. Comparing electrical energy storage technologies regarding their material and carbon footprint. *Energies*, 11(12), 2018.

[58] L. Xingjun, S. Zhiwei, C. Hongping, and B. O. Mohammed. A new fuzzy-based method for load balancing in the cloud-based Internet of things using a grey wolf optimization algorithm. *Int. J. Commun. Syst.*,33(8):1–19, 2020. https://doi:10.3390/en11123386.

[59] K. P. Wong and Z. Dong. Differential Evolution, an Alternative Approach to Evolutionary Algorithm. 73–83, 2005.

[60] A. Naderipour and H. Kamyab. Optimal design of hybrid grid-connected photovoltaic/ wind/battery sustainable energy system improving reliability, cost and emission. *Energy*, 257:124679, 2022. https://doi.org/10.1016/j.energy.2022.124679.

[61] M. Kharrich, S. Kamel, M. Abdel-akher, and A. Eid. Optimization based on movable damped wave algorithm for design of photovoltaic/wind/diesel/biomass/battery hybrid energy systems. *Energy Reports*, 8:11478–11491, 2022. https://doi:10.1016/j.egyr.2022.08.278.

[62] L. Xu, X. Ruan, C. Mao, B. Zhang, and Y. Luo. An improved optimal sizing method for wind-solar-battery hybrid power system. *IEEE Trans. Sustain. Energy*, 4(3):74–785, 2013. https://doi:10.1109/TSTE.2012.22 28509.

[63] K. Vamba, O. Bode, and M. M. Gamil. A scenario-based multi-attribute decision making approach for optimal design of a hybrid off-grid system. *Energy*, 265:125663, 2023. https://doi.org/10.1016/j.energy.2022. 125663.

Biographies

Subhash Yadav, received his B.Tech degree in electrical engineering from B.C. Roy Engineering College Durgapur, India and M.Tech degree from Indian Institute of Technology Roorkee. He is currently pursuing his PhD Degree from NIT Kurukshetra. His research interest includes Renewable Energy Systems and Energy Management.

Pradeep Kumar, received the B.E degree in electrical engineering from G. B. Pant Engineering College Pauri Garhwal, India, in 2009, and the

M.Tech. and PhD degrees from MNNIT Allahabad in 2011 and 2016 respectively. Currently, he is an Assistant Professor in the Department of Electrical Engineering at National Institute of Technology (NIT) Kurukshetra, Haryana, India. His research interests include Energy Management and Power System Monitoring.

Ashwani Kumar, received the B.Tech degree in Electrical Engineering from G. B. Pant University, Pant Nagar, India, in 1988, M.Tech. degree in power systems from Punjab University, Chandigarh, India, in 1994 and Ph.D degree from Indian Institute of Technology, Kanpur, India. Currently, he is a Professor in the Department of Electrical Engineering at National Institute of Technology (NIT)-Kurukshetra, Haryana, India. His research interests include power system deregulation optimization and power system dynamics.